Journal of Materials Chemistry C

PAPER

View Article Online
View Journal | View Issue

Cite this: J. Mater. Chem. C, 2017, 5, 4645

Broad range energy absorption enabled by hydrogenated TiO_2 nanosheets: from optical to infrared and microwave†

Lihong Tian,[ab] Jilian Xu,[c] Michael Just,[a] Michael Green,[a] Lei Liu [c] and Xiaobo Chen *[a]

Received 20th March 2017,
Accepted 18th April 2017

DOI: 10.1039/c7tc01189j

rsc.li/materials-c

Efficient energy harvesting is critical in developing various future clean energy sources and technologies from our ultimate clean energy source – the Sun, which covers a broad range of photon energies ranging from ultraviolet, to visible, infrared, and microwave regions. Absorption is the first key step in the uptake of solar energy for various energy conversions and utilizations. Materials with broad-range electromagnetic interaction are therefore highly desirable. Here, we demonstrate that such broad-range energy absorption from visible light to microwave regions can be achieved with hydrogenated TiO_2 nanosheets. A large near-infrared and visible-light absorption (>60%), a broad mid-IR absorption, and a highly efficient absorption in the microwave region have been obtained with hydrogenated TiO_2 nanosheets. In contrast, barely any absorption is observed for pristine TiO_2 nanosheets in these regions. Therefore, this study shows that with such high absorption across such a broad energy range, hydrogenated TiO_2 nanosheets obviously have a large capability of absorbing solar energy across a broad energy region, which can be potentially useful for various photo, photoelectric, photochemical applications, such as semiconductor devices, photocatalysis, photovoltaics, infrared detection, microwave communication, *etc.*

Introduction

The ability to efficiently harvest energy from solar radiation is critical for the development of future clean energy sources and technologies. One of the keys to effectively utilize solar energy is developing materials that effectively absorb it. Solar energy covers a broad range of photon energies from ultraviolet to visible, infrared, and microwave regions. Absorption is the first key step in the uptake of solar energy for various energy conversions and utilizations. Materials with broad-range electromagnetic interaction are highly desirable for numerous optoelectronic and photo, electric, and chemical applications, such as photocatalysis, photovoltaics, thermoelectronics, *etc.* Enhancing light–matter interaction or absorption over a broad range of energies has a vital importance in the fundamental understanding and numerous practical applications of electromagnetic radiation, such as in semiconductor devices,[1] photocatalysis,[2–4] photovoltaics,[5] infrared (IR) detection,[6] microwave communications,[7] *etc.* However, realization of simultaneous efficient absorption of light across a broad energy range is very challenging since the absorption in different energy regions traditionally requires different mechanisms.[1] It is apparent that new concepts and approaches are needed in order to overcome such a challenge. Hereby, we demonstrate such an attempt to realize efficient light absorption of hydrogenated TiO_2 nanosheets over a broad energy range (3.0–0.00001 eV), from visible-light to IR, and microwave.

Typically, the absorption of ultraviolet radiation (UV, >3.0 eV) requires either molecular ionization, the ejection of electrons when the supplied energy is larger than the ionization energy, or transitions of electrons from ground state to higher electronic states within the atoms or molecules.[1,2] The absorption of visible light (1.7–3.0 eV) typically involves the excitation of electrons to higher energy levels within molecular species or semiconductors.[1] For semiconductors, the absorption of light (with energy larger than their bandgaps) promotes electrons from the valence band to the conduction band, generating excited electrons in the conduction band and holes in the valence band,[1–5] which subsequently can be transported to external circuits to produce electricity in photovoltaic devices or transferred to adjacent molecules to induce reduction/oxidation reactions in photochemical cells.[3,4] The larger the absorption, the higher the electrical current or the photocatalytic activity.[3,4] For example, TiO_2 has been widely

[a] Department of Chemistry, University of Missouri – Kansas City, Kansas City, Missouri 64110, USA. E-mail: chenxiaobo@umkc.edu
[b] Hubei Collaborative Innovation Center for Advanced Organochemical Materials, Hubei University, Wuhan, 430062, China
[c] State Key Laboratory of Luminescence and Applications, Changchun Institute of Optics, Fine Mechanics and Physics, Chinese Academy of Sciences, Changchun, 130033, People's Republic of China

† Electronic supplementary information (ESI) available. See DOI: 10.1039/c7tc01189j

studied as a photocatalyst for renewable energy and sustainable environment applications such as in water splitting, hydrogen generation, and environmental pollutant removal, among others.[2–4] However, its relatively large bandgap (3.0–3.2 eV) results in primarily UV-only optical absorption and thus it has a low overall efficiency of using natural sunlight, where UV only accounts for less than 5% of the total available energy.[8,9] Improving the optical absorption of TiO_2 has been the target of many research efforts such as doping with metal/non-metal elements,[8–10] coupling with narrow bandgap semiconductors or molecules,[11,12] engineering crystal facets,[13–15] and altering lattices of crystalline nanoparticles by hydrogenation or chemical reduction.[16–22] The extension of electromagnetic absorption in TiO_2 to the near infrared region by hydrogenation has been treated as a breakthrough among the efforts towards higher photocatalytic and photoelectrochemical activities in photocatalysis.

Normally, the absorption of infrared radiation (henceforth IR, 10^{-3} to 1.7 eV range) requires transitions from the ground state to excited states of molecular vibrations and results in heating.[1,23] Metals with high thermal conductivity can absorb or reflect IR radiation (heat) quickly as the quantum states of their vibrations lies within this region, although most metals reflect almost all IR radiation.[1,6,24] Highly efficient thermal detection devices can be realized by increasing the IR absorbing capability.[6,24]

The absorption of microwave radiation (10^{-5} to 10^{-3} eV) by molecules typically involves excited rotational states of molecules with electric diploes, subsequently producing heat as a consequence of the resulting intermolecular frictions.[25–27] This absorption leads to the loss of electrical and magnetic fields within the materials, due to the dielectric relaxation effects of dipole rotation associated with the alignment of polar groups (permanent and induced dipoles) and ferromagnetic resonance from strongly interacting electron spins in magnetic domain walls, respectively.[25–27] Conductors strongly absorb both microwave radiation and any lower frequency radiation and generate electric currents and heat the materials.[25–27] For practical applications, efficient microwave absorption is key to avoid detection of aircrafts by radar, and to reduce data and information leakage in various electronic devices.[25–28]

Currently, there seldom exists any material that can efficiently absorb the electromagnetic radiation across such a broad energy range from visible-light to microwave. Here, we show that enhanced absorption in such a broad energy region can be achieved with TiO_2 nanosheets by hydrogenation-induced alterations. Absorption in the visible-light region has been successfully improved ($>60\%$ absorption from 400 to 1000 nm), although no visible-light absorption is seen for pristine TiO_2 nanosheets; absorption in the IR region has been enhanced in a broad range (<4000 cm^{-1}), while only a narrow IR absorption (<1000 cm^{-1}) is observed from the lattice for pristine TiO_2 nanosheets; and considerable absorption in the microwave region has been achieved ((RL (dB)) value of -52.5 or 99.999% absorption) with frequency tunability, but only a poor microwave absorption (RL (dB) value of -3.0) is observed for pristine TiO_2 nanosheets. Thus, this study demonstrates that the light–matter interactions of TiO_2 nanomaterials regarding electromagnetic irradiation can be largely enhanced by hydrogenation over a broad range of energies, which enriches our knowledge for better utilization of electromagnetic energy for various applications.

Results and discussions

Our previous studies on hydrogenated black TiO_2 nanoparticles revealed that hydrogenation induced structural distortions within the outer layers of the nanocrystals result in the formation of disordered structures, and the size of the crystalline phase slightly decreased after hydrogenation.[16,18] The microstructure and crystallinity of both pristine and hydrogenated TiO_2 nanosheets were first analyzed using transmission electron microscopy (TEM). Previous studies have found that crystalline-disordered core–shell structures were formed after hydrogenation in high-resolution transmission electron microscopy (HRTEM) studies, and structural deviations from the standard lattice were readily seen in the outer layer, where bent lattices and non-uniform plane distances were observed near the edge of the nanoparticles.[16,18,29] Cloudy diffraction patterns obatined by electron diffraction and fast Fourier transform (FFT) analyses of hydrogenated TiO_2 nanoparticles revealed an amorphous structure from the crystalline phase.[20,30] Fig. 1A shows that the average length of the pristine TiO_2 nanosheets was around 100 nm. The XRD analysis suggested their average crystalline grain size was 29.0 nm in length [(100) direction]. This meant that these TiO_2 nanosheets were made of many small crystalline grains. The HRTEM image in Fig. 1B shows that these TiO_2 nanosheets were highly crystallized, with well-resolved lattice fringes and clearly seen crystal edge. On the contrary, as seen from Fig. 1C, the average size of the hydrogenated TiO_2 nanosheets was similar to that of the pristine TiO_2 nanosheets, around 100 nm. The crystalline grain size was 26.4 nm in length [(100) direction] for hydrogenated TiO_2 nanosheets. Thus, the hydrogenated TiO_2 nanosheets were made of smaller crystalline grains, similar to pristine TiO_2 nanosheets. The HRTEM in Fig. 1D of hydrogenated TiO_2 nanosheets reveals a layer of amorphous/disordered phase near the surface covering the crystalline core with clear lattice fringes. This observation was consistent with our previous studies on hydrogenated TiO_2 nanoparticles.[16,18,30] It is apparent that hydrogenation induced some structural reorganization near the surface resulting in the formation of some disordered structures. These structures may contain defects leading to a large luminescent background in the Raman spectrum of hydrogenated TiO_2 nanosheets.

Lattice contraction in the disordered layer in hydrogenated TiO_2 nanoparticles was reported,[18,29,31] and was reflected in the X-ray diffraction (XRD) pattern by the shifting of diffraction peaks to higher diffraction angles.[18,32] The XRD patterns of the pristine and hydrogenated TiO_2 nanosheets studied here are shown in Fig. 2A. Clearly, both these samples were highly crystalline, based on their strong diffraction peaks. The average crystalline grain size can be calculated using the Scherrer

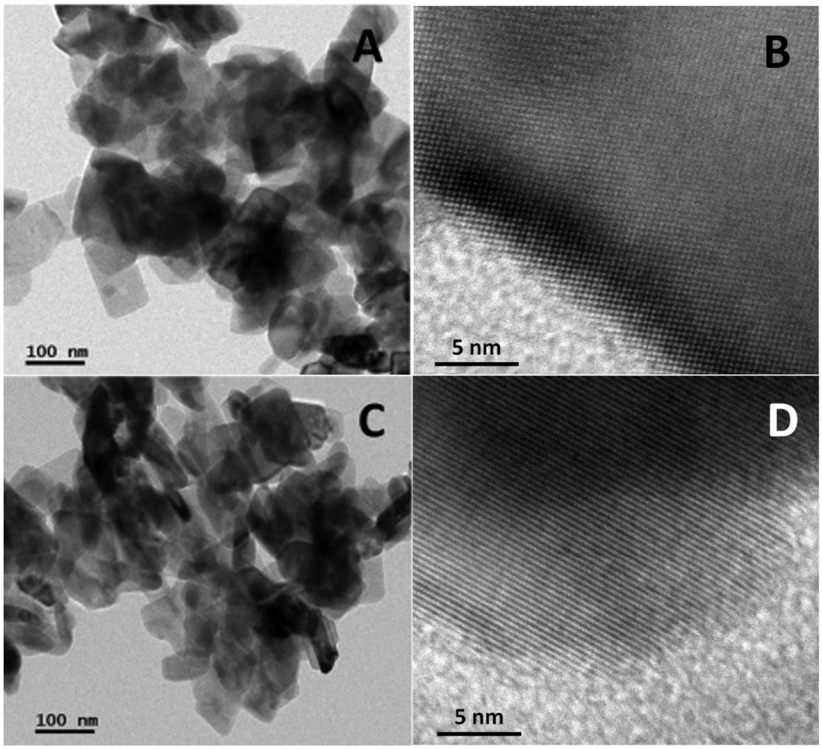

Fig. 1 TEM images of pristine (A and B) and hydrogenated (C and D) TiO_2 nanosheets.

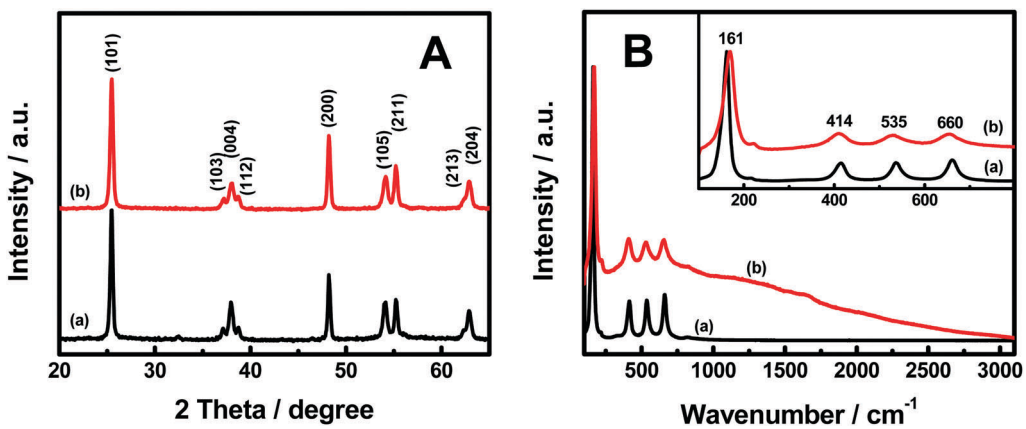

Fig. 2 (A) XRD patterns and (B) Raman spectra of (a) pristine and (b) hydrogenated TiO_2 nanosheets.

equation: $\tau = (K\lambda)/(\beta \cos \theta)$, where τ is the mean size of the ordered (crystalline) domains, which may be smaller or equal to the grain size, K is the shape factor with a typical value of 0.9, λ is the X-ray wavelength, β is the line broadening full width at half maximum (FWHM) peak height in radians, and θ is the Bragg angle.[16,18] Using the FWHM values of the (004) and (200) peaks, we obtained crystalline grain sizes of 16.8 nm and 29.0 nm for pristine TiO_2 nanosheets, and 13.4 nm and 26.4 nm for hydrogenated TiO_2 nanosheets, in the [001] and [100] directions, respectively. Moreover, the average size of the crystalline grains in the hydrogenated TiO_2 nanosheets was slightly smaller than that of the pristine TiO_2 nanosheets. Based on our previous studies,[16,18] some amorphous phase was likely formed outside the crystalline phases of TiO_2 nanosheets after hydrogenation.

Raman studies on hydrogenated TiO_2 nanoparticles revealed that after hydrogenation, the scattering peaks of TiO_2 became much weaker in intensity,[16,32,33] broader in width,[34,35] and had higher values of wavenumbers,[34–36] due to the disordering of the TiO_2 lattice after hydrogenation. The Raman spectra of pristine and hydrogenated TiO_2 nanosheets in this study are shown in Fig. 2B. Strong and sharp Raman peaks at 161, 414, 535, and 660 cm^{-1} were observed for pristine TiO_2 nanosheets. These peaks were attributed to the lattice vibrations in the crystalline anatase phase from the Ti–O bond stretching modes E_g (660 cm^{-1}), B_{1g} (519 cm^{-1}) and A_{1g} (513 cm^{-1}), and the

O–Ti–O bending modes B_{1g} (414 cm^{-1}) and E_g (164 cm^{-1}).[16] After hydrogenation, these Raman peaks became weaker and broader. In addition, the E_g mode of the O–Ti–O bond shifted to a higher wavenumber (169 cm^{-1}) after hydrogenation. These were consistent with previous studies of hydrogenated TiO_2 nanoparticles.[16,30] Moreover, a large luminescent background, most likely due to defects, appeared after hydrogenation. Such observations indicated that defects were induced within the nanosheets by the hydrogenation process.

Based on the above structural analysis, partially disordered structures likely in the form of crystalline core/disordered shell structures were formed by hydrogenation of TiO_2 nanosheets and even the starting pristine TiO_2 nanosheets were highly crystallized. These structural alterations may lead to a change in the bonding structures of TiO_2 nanosheets, *e.g.* the couplings between the oxygen 2p and the titanium 3d orbitals, inducing a change in the light–matter interactions of TiO_2 nanosheets, as reflected by the change in their absorption of electromagnetic radiation across the broad range of energies.

Our previous discovery of black TiO_2 nanoparticles by hydrogenation showed that the optical bandgap of TiO_2 narrowed down to around 1.5 eV (850 nm) with the onset of absorption near 1.0 eV (1200 nm) from around 3.3 eV (375 nm).[16] This large shift in the bandgap was attributed to the stabilized disordered lattice in the crystalline core/disordered shell structures induced by hydrogenation, which altered the coupling of the oxygen 2p and titanium 3d orbitals in the valence band.[16] The increase of the optical absorption was beneficial for the photocatalytic activity of TiO_2 nanoparticles.[16,37] Hydrogenated TiO_2 nanomaterials have shown improved photocatalytic activity in hydrogen generation,[16,34] photo-oxidation of water,[38] and photodecomposition of 2,4-dichlorophenol,[39] methylene blue,[16,32] methyl-orange[37] and acetaldehyde.[40] Thus, the large enhancement of the optical absorption in this region is important.

The UV-visible spectra of pristine and hydrogenated TiO_2 nanosheets are shown in Fig. 3A. Pristine TiO_2 nanosheets displayed almost 100% reflection of visible and near-infrared light and absorbed only ultraviolet (UV) light below 400 nm, similar to that of pure TiO_2 nanoparticles.[16] However, hydrogenated TiO_2 nanosheets absorbed more than 60% light from 400 nm to 1000 nm, besides the large UV absorption similar to pristine TiO_2 nanosheets. Obviously, the hydrogenation process increased the absorption of TiO_2 nanosheets in the visible-light region. This was consistent with our previous finding of hydrogenated black TiO_2 nanoparticles.[16]

A broad IR absorption has been observed from the lattice of hydrogenated TiO_2 nanosheets. The infrared absorption (4000–600 cm^{-1}, 0.5–0.07 eV) was measured using Fourier transform infrared (FTIR) spectroscopy. In previous studies, the changes in the IR absorption caused by the hydrogenation on TiO_2 nanomaterials were found to be related to the surface OH groups and largely depended on the hydrogenation condition.[29,32,37,39,41] For example, less OH groups were seen in hydrogenated TiO_2 microspheres treated at 500 °C for 4 h under a flow of H_2 (5% in N_2, 300 sccm)[39] and at 450 °C for 1 h in a 5% H_2 and 95% Ar atmosphere, compared to the starting pristine TiO_2 nanomaterials.[41] However, more surface OH groups were observed on TiO_2 nanosheets hydrogenated at 400 °C for 2 h under a 10 bar pure H_2 atmosphere,[32] and treated with hydrogen plasma at 500 °C for 4–8 h.[37] Fig. 3B shows the FTIR spectra of pristine and hydrogenated TiO_2 nanosheets in this study. Pristine TiO_2 nanosheets showed a weak but broad absorption band near 3300 cm^{-1} and a sharp absorption band below 1000 cm^{-1}. The broad band centered at 3300 cm^{-1} was due to the O–H stretching vibrations of strongly adsorbed H_2O,[42,43] and the sharp absorption band below 1000 cm^{-1} was likely due to the vibrations of Ti–O bonds.[42,43] However, hydrogenated TiO_2 nanosheets had very different FTIR spectral features. The broad bands ascribed to the vibrations of O–H on the surface disappeared. Instead, a broad background-like absorption appeared. This phenomenon is different from previous observation.[29,32,37,39,41] The broad and featureless IR absorption of the hydrogenated TiO_2 nanosheets could be attributed to the possible defects (*e.g.* oxygen vacancy or free electrons, hydrogen dopant) associated with the disordered lattice of the hydrogenated TiO_2 nanosheets.[44] More importantly,

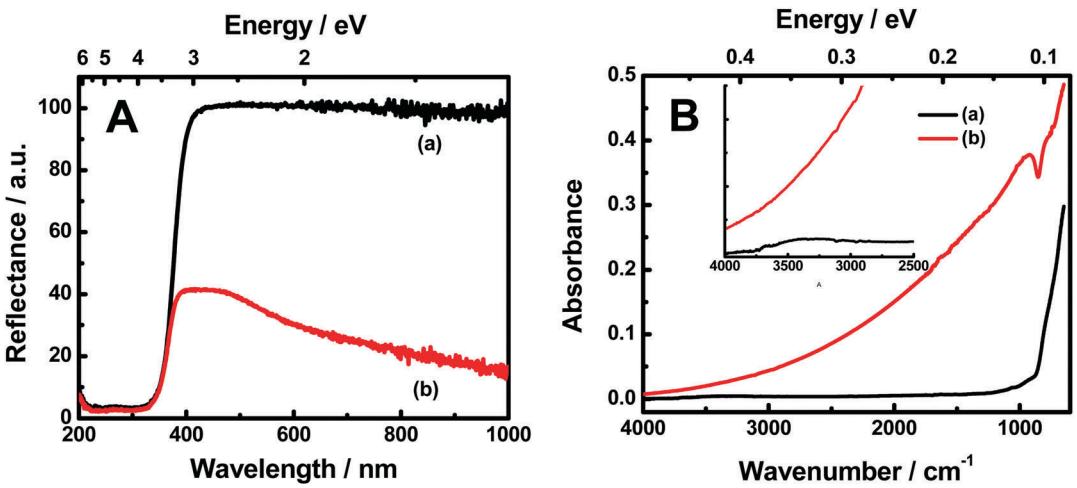

Fig. 3 (A) UV-visible and (B) FTIR spectra of (a) pristine and (b) hydrogenated TiO_2 nanosheets.

this absorption increased monochromatically as the radiation frequency decreased. This suggested that the number of defects increased when their energies became smaller. This broad and large IR absorption from the defects in the hydrogenated TiO_2 lattice was consistent with the large luminescent background in the Raman spectra. Thus, a broad IR absorption from the lattice of TiO_2 nanosheets has been obtained by hydrogenation. As shown, this broad, continuous and featureless IR absorption from the lattice defects (likely more coupled with each other) is different from the commonly seen absorption due to OH vibrations (likely less coupled with each other), which normally shows up with a relatively much weaker and narrower band near 3300 cm^{-1}, as can be seen from the IR spectrum of the pristine TiO_2 nanosheets in the inset of Fig. 3B.

Although it has a large static dielectric constant, TiO_2 has a poor response in the microwave region due to its lack of traditional microwave absorbing mechanisms such as dipole rotation and ferromagnetic resonance. In order to measure its absorption capability in the microwave region, its dielectric properties such as complex permittivity (ε) and permeability (μ) were measured. The real parts ε' and μ' are related to the stored electrical and magnetic energy within the material. The imaginary parts ε'' and μ'' are related to the dissipation (or loss) of electrical and magnetic energy.[1,8] Large changes in the complex permittivity (ε) and permeability (μ) values, ε', ε'', μ', and μ'', were seen in TiO_2 nanosheets after hydrogenation, due to the changed orbital couplings in the disordered TiO_2 lattice.

We have demonstrated previously that the dielectric constants of TiO_2 nanoparticles can be largely modified with the alterations of their local structural features *via* induced disorder in the outer layer of crystalline nanoparticles.[30,45,46] The structural alterations perturb both the electronic couplings between the titanium 3d and oxygen 2p orbitals and the internal lattice potentials across the nanoparticles. In addition, transit or permanent charge accumulation or polarization can be expected along the interfaces between the crystalline and disordered phases to create internal built-in electric fields within the nanoparticles. The propagation of the introduced electromagnetic field can echo those electric field to possibly induce larger interactions within the TiO_2 media to have larger dielectric constants.[30,45,46] Changes in the ε' values were observed from 6.1–6.5 for normal TiO_2 nanoparticles to 17–25 for hydrogenated TiO_2 nanoparticles, a 4.3-fold difference was caused by hydrogenation. Fig. 4A shows the real

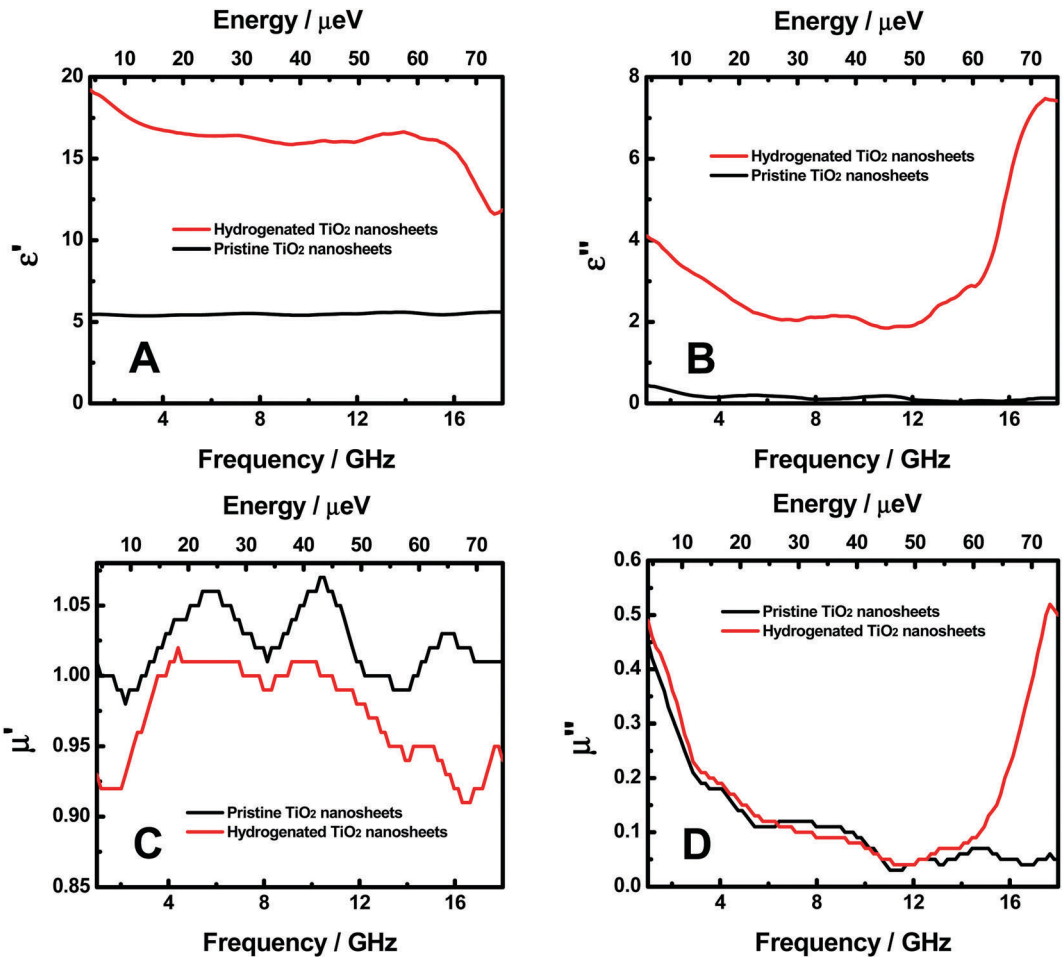

Fig. 4 Frequency dependence of (A) the real part (ε') and (B) the imaginary part (ε'') of the complex permittivity, (C) the real part (μ') and (D) the imaginary part (μ'') of the complex permeability in the microwave region of pristine and hydrogenated TiO_2 nanosheets.

part ε' of complex permittivity for pristine and hydrogenated TiO_2 nanosheets/wax composites in this study. For these measurements, TiO_2 nanosheets were dispersed in melted paraffin wax. Pristine TiO_2 nanosheets/wax composites displayed a relatively constant value of around 5.5 for ε' in the frequency range of 1.0–18.0 GHz. With the same TiO_2 loading (60 wt%), pristine TiO_2 nano particle/wax composites exhibited ε' values of 6.1–6.5 in the same frequency range.[30,45] Apparently, TiO_2 nanoparticles exhibited larger ε' values compared to the TiO_2 nanosheets. This indicated that the morphology of the TiO_2 nanomaterials had an important influence on their dielectric properties. The difference in the dielectric constants of TiO_2 nanoparticles and nanosheets can be attributed to the differences in charge distribution and density along various crystal directions in TiO_2. TiO_2 has a larger charge density along the $\langle 001 \rangle$ direction, and a smaller charge density along the $\langle 100 \rangle$ and $\langle 010 \rangle$ directions. Thus, the electromagnetic interaction of microwave radiation with TiO_2 and the induced electric relaxation is larger in the $\langle 001 \rangle$ direction than in the $\langle 100 \rangle$ or $\langle 010 \rangle$ direction. The shorter length along $\langle 001 \rangle$ direction and longer length along the $\langle 100 \rangle$ and $\langle 010 \rangle$ directions of (001) faceted TiO_2 nanosheets thus induces a smaller electromagnetic interaction in the nanosheets than in the nanoparticles. Hydrogenated TiO_2 nanosheet/wax composites showed much higher ε' values than pristine TiO_2 nanosheet/wax composites. Their ε' values decreased gradually from 19.2 at 1.0 GHz to 16.0 at 15.4 GHz and then to 11.7 at 18.0 GHz. Compared to hydrogenated TiO_2 nanoparticle/wax composites, hydrogenated TiO_2 nanosheet/wax composites showed slightly smaller ε' values, due to the shorter length in the high charge density $\langle 001 \rangle$ direction of the nanosheets. As the ε' value of the epoxy was 2.5 at the X-band frequency,[47] the ε' value of the hydrogenated TiO_2 nanosheets was thus estimated to be about 4.5 times higher than that of the pristine TiO_2 nanosheets in the frequency range of 1.0–18.0 GHz. Apparently, a much higher efficiency of storing electric energy was achieved with hydrogenated TiO_2 nanosheets than with the pristine TiO_2 nanosheets. The improvement of the electromagnetic interaction can be attributed to the increased charge density along the $\langle 001 \rangle$ direction and the disorder alteration caused by hydrogenation as seen from the TEM images. Hydrogenation apparently changed the orbital couplings in TiO_2 and the charge density along various directions by introducing disorders around the crystalline core. Hydrogenated TiO_2 nanosheet/wax composites exhibited a slightly higher improvement (4.5-fold *vs.* 4.3-fold) than hydrogenated TiO_2 nanoparticle/wax composites, compared to the pristine nanomaterial/wax composites. Thus, this suggested that the alteration of the charge density along the $\langle 001 \rangle$ direction in the TiO_2 nanosheets was more obvious than in other directions by hydrogenation.

Fig. 4B shows the imaginary part ε'' of complex permittivity for pristine and hydrogenated TiO_2 nanosheet/wax composites. Pristine TiO_2 nanosheet/wax composites showed relatively constant ε'' values of 0.03–0.1 in the frequency range of 1.0–18.0 GHz. In our earlier study, TiO_2 nanocrystals/epoxy composites showed ε'' values of 0.03–0.3 in the same frequency range.[30,45] This was likely due to the larger electrical relaxation along the $\langle 001 \rangle$ direction than the $\langle 100 \rangle$ and $\langle 010 \rangle$ directions in TiO_2. Hydrogenated TiO_2 nanosheets/wax composites showed much higher ε'' values in the same frequency range. The ε'' value decreased gradually from 4.1 at 1.0 GHz to 1.8 at 11.0 GHz and then increased to 7.4 at 18.0 GHz. The average was around 3.5. As the epoxy showed ε'' values of 0–0.02 at the X-band frequency,[47] hydrogenated TiO_2 nanosheets had 70 times higher ε'' values than the pristine TiO_2 nanosheets. This suggested that hydrogenated TiO_2 nanosheets were more efficient in dissipating electrical energy under the electromagnetic field. This enhancement was likely due to the larger relaxation of electrical energy into heat as the hydrogenated TiO_2 nanosheets had disordered structures which can effectively convert electromagnetic radiation into thermal energy. The comparison of the dielectric dissipation factor, $tg\delta_\varepsilon = \varepsilon''/\varepsilon'$, which measures how much electric power is lost in a material *versus* how much is stored,[30,45] shown in Fig. S1 (ESI†), also displayed that hydrogenated TiO_2 nanosheets had a higher efficiency of dissipating electrical energy of the microwave radiation with a 10-fold increase in the $tg\delta_\varepsilon$ value compared to the pristine TiO_2 nanosheets.

To understand how the samples responded to the magnetic component of the microwave radiation, we also measured their permeability. Permeability in electromagnetism is the measure of the ability of a material to support the formation of a magnetic field within itself, or the degree of magnetization that a material acquiresin response to an applied magnetic field. The complex permeability of a material contains the real part μ' and the imaginary part μ''. μ' is related to the stored magnetic energy within the medium, and μ'' is related to the dissipation (or loss) of magnetic energy within the medium. Fig. 4C shows the real part μ' of complex permeability for pristine and hydrogenated TiO_2 nanosheets. The μ' of the pristine TiO_2 nanosheets increased slowly from 0.95 at 1.0 GHz to 1.03 at 6.0 GHz, then decreased to 1.00 at 8.0 GHz, increased to 1.03 at 11.0 GHz, and stayed around 1.03 until 18.0 GHz. The μ' of the pristine TiO_2 nanosheets was higher than that of the pristine TiO_2 nanoparticles (0.93–1.02). The μ' of hydrogenated TiO_2 nanosheets was lower than that of the pristine TiO_2 nanosheets. It increased slowly from 0.92 at 1.0 GHz to 1.01 at 6.0 Hz and then slowly decreased to 0.92 at 18.0 GHz. The μ' of hydrogenated TiO_2 nanoparticles was found to be 0.80–0.99 in our previous studies. Thus, hydrogenated TiO_2 nanosheets had a slightly larger μ' than hydrogenated TiO_2 nanoparticles. Fig. 4D displays the imaginary part $\mu''$of complex permeability for pristine and hydrogenated TiO_2 nanosheets. The μ'' values for pristine TiO_2 nanosheets decreased as the frequency increased from about 0.45 at 1.0 GHz to 0.05 at 18.0 GHz. The μ'' values of hydrogenated TiO_2 nanosheets were similar within the frequency region of 1–12.0 GHz, decreasing from 0.50 at 1.0 GHz to 0.05 at 12.0 GHz, but were much higher within 12.0–18.0 GHz, increasing from 0.05 at 12.0 GHz to 0.50 at 18.0 GHz. The small influence of hydrogenation on the permeability of the TiO_2 nanosheets in the lower frequency range (1–12.0 GHz) was similar to that on the TiO_2 nanoparticles as we found previously.[30,45] That was attributed to the little impact of hydrogenation on the creation of possible transit or permanent magnetic species in TiO_2. In our previous

studies on hydrogenated TiO_2 nanoparticles, no oxygen vacancies or Ti^{3+} defects were observed, thus offering little paramagnetic resonance.[30,45] However, the apparent sharp increase of the μ'' values in the frequency range of 12.0–18.0 GHz hinted that some paramagnetic resonance may be induced due to the possible creation of oxygen radicals or other paramagnetic species by hydrogenation, as summarized in a review article on hydrogenated TiO_2 nanomaterials.[22] The increase of the μ'' values indicated that hydrogenation increased the magnetic dissipation through absorption, or in other words, the increased integral of the product of the initial and end states with the magnetic absorption matrix or cross-section coefficient, which might be due to the increase of each component or one of these components. As shown in Fig. S2 (ESI†), the comparison of the magnetic dissipation factor, $tg\delta_\mu = \mu''/\mu'$, which measures how much magnetic power is lost in a material *versus* how much is stored,[25–27] also indicated that hydrogenated TiO_2 nanosheets had a much higher efficiency of dissipating magnetic energy in the high frequency region.

In brief, the complex permittivity (ε) and permeability (μ) values, ε', ε'', μ', and μ'', of TiO_2 nanosheets in the microwave region were largely changed after hydrogenation, due to the perturbed orbital couplings in the disordered TiO_2 lattice. Higher efficiency was observed for storing and dissipating the electrical energy of the microwave electromagnetic field in TiO_2 nanosheets after hydrogenation, with higher dissipation efficiency of magnetic energy in high frequency ranges. These may lead to a higher efficiency of absorbing microwave radiation.

The microwave reflection loss (RL) curve can be calculated according to the following equations:

$$Z_{in} = Z_0(\mu_r/\varepsilon_r)^{1/2}\tanh[j(2\pi fd/c)(\mu_r\varepsilon_r)^{1/2}] \quad (1)$$

$$\mathrm{RL\ (dB)} = 20\log|(Z_{in} - Z_0)/(Z_{in} + Z_0)| \quad (2)$$

$$\mathrm{RL\ (dB)} = 10\log_{10}(P_i/P_r) \quad (3)$$

where f is the frequency of the electromagnetic wave, d the thickness of the absorber, c the velocity of light, Z_0 the impedance of free space, Z_{in} the input impedance of the absorber, RL (dB) the reflection loss in dB, P_i the incident power, and P_r the reflected power.[48,49] From eqn (3), a RL value less than −30 corresponds to a 99.9% reflection loss or absorption. This suggests that a material with a RL value less than −30 can absorb 99.9% irradiation power, and can be treated as a proficient absorber.

According to eqn (1) and (2), the calculated RL curves of the pristine and hydrogenated TiO_2 nanosheets with a thickness of 3.0 mm are shown in Fig. 5A. Pristine TiO_2 nanosheets exhibited a RL (dB) value of −1.0 in most regions in the range of 1.0–18.0 GHz. That only corresponded to 20.6% absorption. On the other hand, hydrogenated TiO_2 nanosheets showed very negative RL (dB) values in the range of 1.0–18.0 GHz with a valley value of −37.9 at around 13.9 GHz. This suggested that a much larger reflection loss of microwave radiation was achieved with TiO_2 nanosheets by hydrogenation treatment. That loss corresponded to 99.99% absorption. The enhanced microwave absorption of hydrogenated TiO_2 nanosheets can be explained by the innovative collective-movement-of-interfacial-dipole mechanism that was proposed in our previous studies.[30,45] Hydrogenation induced large structural and chemical changes in TiO_2 nanosheets as revealed by Raman and TEM observations. Some of the crystalline phases converted into amorphous phases, and were possibly doped with hydrogen.[29] Evidently, the corresponding electronic structures or thus the dielectric constants of these regions were different from those of the crystalline TiO_2 regions.[30,45] Usually, charge accumulation was expected in the phase boundaries, causing collective interfacial dipoles along the interfaces. The propagation of the microwave electromagnetic field through the material caused rapid rotation of the polarizing direction at these interfaces. Therefore, enhanced microwave absorption was obtained. Similar improvements in microwave absorption have also been observed for hydrogenated TiO_2 nanoparticles.[30,45] However, unlike in the hydrogenated TiO_2 nanoparticles, the permeability (μ) values were barely affected by hydrogenation, in hydrogenated TiO_2 nanosheets, the imaginary part of the permeability value were largely changed by hydrogenation in the high frequency range. So, the contribution of

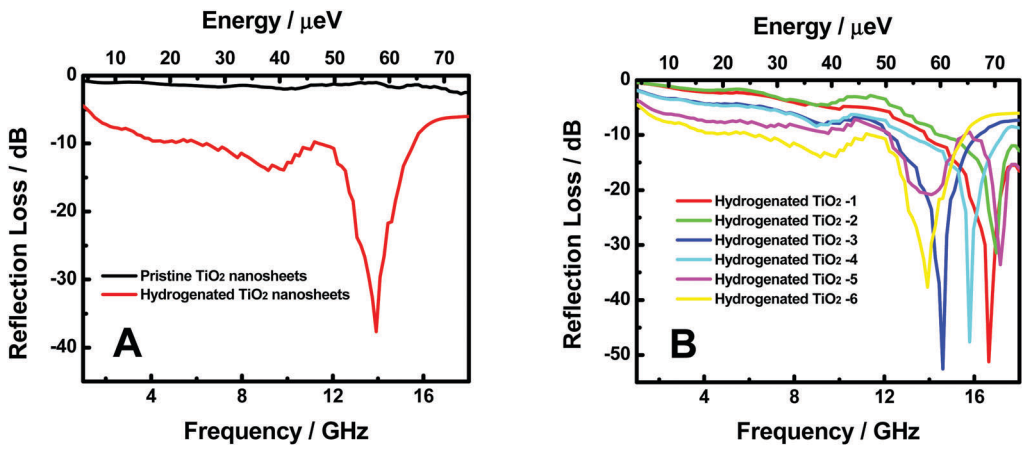

Fig. 5 Frequency dependence of reflection loss in the microwave region of (A) pristine and hydrogenated TiO_2 nanosheets and (B) hydrogenated TiO_2 nanosheets obtained under various hydrogenation conditions.

paramagnetic resonance could not be completely ignored for the microwave absorption in hydrogenated TiO_2 nanosheets.

We further fabricated a series of hydrogenated TiO_2 nanosheets under different hydrogenation conditions, that is, different reaction times. The reaction time has been found to play an important role in changing the optical and structural properties of TiO_2 nanoparticles, as the extent of hydrogenation was apparently dependent on the hydrogenation reaction time.[50,51] Anatase TiO_2 is made of TiO_6 octahedrons slightly distorted from a perfect octahedron. The Ti–O bond length in the apical directions is slightly longer than that in the equatorial directions. Four of the eight neighbors of each octahedron share edges and the others share corners. The corner-sharing octahedra form (001) planes and are connected to their edges with the plane of octahedra below.[17] The charge density along the $\langle 001 \rangle$ direction is higher than that along the $\langle 100 \rangle$ or $\langle 010 \rangle$ direction. And the hydrogenation rates along these directions are different.[50,51] By changing the hydrogenation time, the structural properties of TiO_2 nanosheets and thus their microwave absorption performance can be finely tuned. The RL (dB) curves of the series of hydrogenated TiO_2 nanosheets are shown in Fig. 5B. Their RL (dB) peak values ranged from -31.0 to -52.5, corresponding to absorption larger than 99.9% to 99.999%. Thus, all these hydrogenated TiO_2 nanosheets exhibited excellent microwave absorption performance. The frequency regions of the RL peaks of these hydrogenated TiO_2 nanosheets spanned from 13.9 to 17.2 GHz. As seen, TiO_2 nanosheets hydrogenated under different conditions showed different absorption properties. Or in other words, this demonstrated that the microwave absorption frequency of hydrogenated TiO_2 nanosheets can be adjusted by changing the hydrogenation conditions.

Overall, dramatically enhanced microwave absorption ($>99.999\%$) has been obtained for TiO_2 nanosheets *via* hydrogenation treatment, and the absorption frequency can be adjusted by changing the hydrogenation conditions. The large microwave absorption efficiency with tunable frequency holds promising prospects in anti-reflective coatings for aircraft and anti-leaking coatings for various electronic devices.

Conclusions

Improved absorption over a broad region of the electromagnetic spectrum, ranging from visible light to microwave regions, has been achieved with TiO_2 nanosheets through hydrogenation treatment. We have demonstrated a high capacity for electromagnetic absorption ($>60\%$) across the visible-light and near-infrared regions, a broad IR absorption from the lattice, and up to 99.999% absorption in the microwave region. In contrast, pristine TiO_2 nanosheets barely have any absorption capabilities within these regions. Thus, we have successfully shown that a dramatic improvement of the light–matter interaction over a broad energy range can be achieved by hydrogenation treatment of the otherwise inactive materials. This improvement may hold promising prospects in many fields such as solar cells, photocatalysis, IR sensing, radar dodging, information protection, *etc.* This study therefore may provide a new approach for enhancing our capability to manipulate the properties and applications of materials towards our various needs.

Experimental

Anatase TiO_2 nanosheets were prepared by a hydrothermal method using titanium butoxide and concentrated hydrofluoric acid solution.[17,18] The precipitates were filtered, washed with D. I. water, and dried. Pristine TiO_2 nanosheets were obtained by calcining these precipitates at 500 °C for 6 hours in air. Hydrogenated TiO_2 nanosheets were obtained by heating pristine TiO_2 nanosheets at 500 °C for 6 hours under hydrogen atmosphere. To demonstrate the tunability of the frequency of the microwave absorption, a series of hydrogenated TiO_2 nanosheets were obtained by heating pristine TiO_2 nanosheets at 500 °C for 1–6 hours under hydrogen atmosphere and named hydrogenated TiO_2-1, 2, 3, 4, 5 and 6, respectively.

X-ray diffraction (XRD) was performed using a Rigaku Miniflex XRD instrument with Cu Kα radiation as the X-ray source (wavelength = 1.5418 Å). The Raman spectra were collected on an EZRaman-N benchtop Raman spectrometer with an excitation wavelength of 785 nm. The transmission electron microscopy (TEM) study was performed on a FEI Tecnai F200 TEM. The electron accelerating voltage was at 200 kV. A small amount of sample was dispersed in water, dropped onto a thin holey carbon film, and dried overnight before TEM measurements. The Fourier transform infrared (FTIR) spectra were collected using a Thermo-Nicolet iS10 FT-IR spectrometer with an attenuated total reflectance (ATR) unit. TiO_2 nanoparticles were pressed onto the ZnSe crystal of the ATR unit, and the measurements were performed in air at room temperature.

The complex permittivity and permeability of pristine and hydrogenated TiO_2 nanosheets were measured at the frequency range of 1–18 GHz using a HP8722ES network analyzer. The TiO_2 nanosheets were dispersed in melted paraffin wax, and the mixture was cast into a ring mold with a thickness of 2.0 mm, inner diameter of 3 mm, and outer diameter of 7 mm. The content of TiO_2 nanosheets was 60 wt% in mass, and the testing was performed at room temperature.

Acknowledgements

X. C. appreciates the support from the U.S. National Science Foundation (DMR-1609061), and the College of Arts and Sciences, University of Missouri – Kansas City. L. T. thanks the National Natural Science Foundation of China (No. 51302072) and China Scholarship Council for their financial support. L. L. acknowledges the support of the National Natural Science Foundation of China (No. 11174273).

Notes and references

1 P. Y. Yu and M. Cardona, *Fundamentals of semiconductors: physics and materials properties*, Springer, Berlin, 2001.

2 A. Fujishima and K. Honda, *Nature*, 1972, **238**, 37.
3 X. Chen, S. Shen, L. Guo and S. S. Mao, *Chem. Rev.*, 2010, **110**, 6503.
4 X. Chen, C. Li, M. Grätzel, R. Kostecki and S. S. Mao, *Chem. Soc. Rev.*, 2012, **41**, 7909.
5 M. Gratzel, *Acc. Chem. Res.*, 2009, **42**, 1788.
6 A. Rogalski, *Infrared Detectors*, CRC Press, Florida, 2011.
7 A. R. Von Hippel, *Dielectric Materials and Applications*, Artech House, Boston, 1995.
8 R. Asahi, T. Morikawa, T. Ohwaki, K. Aoki and Y. Taga, *Science*, 2001, **293**, 269.
9 X. Chen and C. Burda, *J. Am. Chem. Soc.*, 2008, **130**, 5018.
10 W. Choi, A. Termin and M. R. Hoffmann, *J. Phys. Chem.*, 1994, **98**, 13669.
11 M. Dahl, Y. Liu and Y. Yin, *Chem. Rev.*, 2014, **114**, 9853.
12 Y. Ma, X. Wang, Y. Jia, X. Chen, H. Han and C. Li, *Chem. Rev.*, 2014, **114**, 9987.
13 H. G. Yang, C. H. Sun, S. Z. Qiao, J. Zou, G. Liu, S. C. Smith, H. M. Cheng and G. Q. Lu, *Nature*, 2008, **453**, 638.
14 F. De Angelis, C. Di Valentin, S. Fantacci, A. Vittadini and A. Selloni, *Chem. Rev.*, 2014, **114**, 9708.
15 G. Liu, H. G. Yang, J. Pan, Y. Q. Yang, G. Q. (Max) Lu and H. M. Cheng, *Chem. Rev.*, 2014, **114**, 9559.
16 X. Chen, L. Liu, P. Y. Yu and S. S. Mao, *Science*, 2011, **331**, 746.
17 L. Liu and X. Chen, *Chem. Rev.*, 2014, **114**, 9890.
18 T. Xia and X. Chen, *J. Mater. Chem. A*, 2013, **1**, 2983.
19 A. Naldoni, M. Allieta, S. Santangelo, M. Marelli, F. Fabbri, S. Cappelli, C. L. Bianchi, R. Psaro and V. Dal Santo, *J. Am. Chem. Soc.*, 2012, **134**, 7600.
20 G. Zhu, T. Lin, X. Lu, W. Zhao, C. Yang, Z. Wang, H. Yin, Z. Liu, F. Huang and J. Lin, *J. Mater. Chem. A*, 2013, **1**, 9650.
21 C. Yang, Z. Wang, T. Lin, H. Yin, X. Lu, D. Wan, T. Xu, C. Zheng, J. Lin, F. Huang, X. Xie and M. Jiang, *J. Am. Chem. Soc.*, 2013, **135**, 17831.
22 X. Chen, L. Liu and F. Huang, *Chem. Soc. Rev.*, 2015, **44**, 1861.
23 J. M. Hollas, *Modern Spectroscopy*, Wiley, New Jersey, 2004.
24 M. Fox, *Optical Properties of Solids*, Oxford University Press, Oxford, 2010.
25 D. Micheli, *Radar absorbing materials and microwave shielding structures design*, LAMBERT Academic Publishing, New York, 2012.
26 A. R. Von Hippel, *Dielectric Materials and Applications*, Artech House, Boston, 1995.
27 Y. Duan and H. Guan, *Microwave Absorbing Materials*, Pan Stanford Publishing, 2017.
28 V. M. Petrov and V. V. Gagulin, *Inorg. Mater.*, 2001, **37**, 93.
29 X. Chen, L. Liu, Z. Liu, M. A. Marcus, W. C. Wang, N. A. Oyler, M. E. Grass, B. Mao, P. A. Glans, P. Y. Yu, J. Guo and S. S. Mao, *Sci. Rep.*, 2013, **3**, 1510.
30 T. Xia, C. Zhang, N. A. Oyler and X. Chen, *Adv. Mater.*, 2013, **25**, 6905.
31 A. Naldoni, M. Allieta, S. Santangelo, M. Marelli, F. Fabbri, S. Cappelli, C. L. Bianchi, R. Psaro and V. Dal Santo, *J. Am. Chem. Soc.*, 2012, **134**, 7600.
32 W. Wang, Y. Ni, C. Lu and Z. Xu, *RSC Adv.*, 2012, **2**, 8286.
33 X. Jiang, Y. Zhang, J. Jiang, Y. Rong, Y. Wang, Y. Wu and C. Pan, *J. Phys. Chem. C*, 2012, **116**, 22619.
34 H. Lu, B. Zhao, R. Pan, J. Yao, J. Qiu, L. Luo and Y. Liu, *RSC Adv.*, 2014, **4**, 1128.
35 L. Zeng, W. Song, M. Li, D. Zeng and C. Xie, *Appl. Catal., B*, 2014, **147**, 490.
36 C. Sun, Y. Jia, X. H. Yang, H. G. Yang, X. Yao, G. Q. (Max) Lu, A. Selloni and S. C. Smith, *J. Phys. Chem. C*, 2011, **115**, 25590.
37 Z. Wang, C. Yang, T. Lin, H. Yin, P. Chen, D. Wan, F. Xu, F. Huang, J. Lin, X. Xie and M. Jiang, *Adv. Funct. Mater.*, 2013, **23**, 5444.
38 S. Hoang, S. P. Berglund, N. T. Hahn, A. J. Bard and C. B. Mullins, *J. Am. Chem. Soc.*, 2012, **134**, 3659.
39 Z. Zheng, B. Huang, J. Lu, Z. Wang, X. Qin, X. Zhang, Y. Dai and M. H. Whangbo, *Chem. Commun.*, 2012, **48**, 5733.
40 A. Danon, K. Bhattacharyya, B. K. Vijayan, J. Lu, D. J. Sauter, K. A. Gray, P. C. Stair and E. Weitz, *ACS Catal.*, 2012, **2**, 45.
41 Z. Lu, C. T. Yip, L. Wang, H. Huang and L. Zhou, *ChemPlusChem*, 2012, **77**, 991.
42 J. Zou, J. Gao and F. Xie, *J. Alloys Compd.*, 2010, **497**, 420.
43 Y. Zhang, M. Shang, Y. Mi, T. Xia, P. Wallenmeyer, J. Murowchick, L. Dong, Q. Zhang and X. Chen, *ChemPlusChem*, 2014, **79**, 1159.
44 M. J. Elser and O. Diwald, *J. Phys. Chem. C*, 2012, **116**, 2896.
45 T. Xia, C. Zhang, N. A. Oyler and X. Chen, *J. Mater. Res.*, 2014, **29**, 2198.
46 T. Xia, Y. Cao, N. A. Oyler, J. Murowchick, L. Liu and X. Chen, *ACS Appl. Mater. Interfaces*, 2015, **7**, 10407–10413.
47 D. L. Zhao, X. Li and Z. M. Shen, *Compos. Sci. Technol.*, 2008, **68**, 2902.
48 M. Matsumoto and Y. Miyata, *IEEE Trans. Magn.*, 1997, **33**, 4459.
49 L. Tian, X. Yan, J. Xu, P. Wallenmeyer, J. B. Murowchick, L. Liu and X. Chen, *J. Mater. Chem. A*, 2015, **3**, 12550–12556.
50 L. Liu, P. P. Yu, X. Chen, S. S. Mao and D. Z. Shen, *Phys. Rev. Lett.*, 2013, **111**, 065505.
51 H. Lu, B. Zhao, R. Pan, J. Yao, J. Qiu, L. Luo and Y. Liu, *RSC Adv.*, 2014, **4**, 1128.